IEEE Access
Multidisciplinary | Rapid Review | Open Access Journal

Received January 21, 2021, accepted February 1, 2021, date of publication February 4, 2021, date of current version February 12, 2021.

Digital Object Identifier 10.1109/ACCESS.2021.3057237

"Pencil Beamforming Increases Human Exposure to ElectroMagnetic Fields": True or False?

LUCA CHIARAVIGLIO[1,2], (Senior Member, IEEE), SIMONE ROSSETTI[1,2], SARA SAIDA[1,2], STEFANIA BARTOLETTI[2,3], (Member, IEEE), AND NICOLA BLEFARI-MELAZZI[1,2]

[1]Department of Electronic Engineering, University of Rome Tor Vergata, 00133 Rome, Italy
[2]Consorzio Nazionale Interuniversitario per le Telecomunicazioni (CNIT), 00133 Rome, Italy
[3]IEIIT, CNR, 40136 Bologna, Italy

Corresponding author: Luca Chiaraviglio (luca.chiaraviglio@uniroma2.it)

This work was supported by the European Union's Horizon 2020 Research and Innovation Programme under Grant 871249.

ABSTRACT According to a very popular belief - very widespread among non-scientific communities - the exploitation of narrow beams, a.k.a. "pencil beamforming", results in a prompt increase of exposure levels radiated by 5G Base Stations (BSs). To face such concern with a scientific approach, in this work we propose a novel localization-enhanced pencil beamforming technique, in which the traffic beams are tuned in accordance with the uncertainty localization levels of User Equipment (UE). Compared to currently deployed beamforming techniques, which generally employ beams of fixed width, we exploit the localization functionality made available by the 5G architecture to synthesize the direction and the width of each pencil beam towards each served UE. We then evaluate the effectiveness of pencil beamforming in terms of ElectroMagnetic Field (EMF) exposure and UE throughput levels over different realistic case-studies. Results, obtained from a publicly released open-source simulator, dispel the myth: the adoption of localization-enhanced pencil beamforming triggers a prompt reduction of exposure w.r.t. other alternative techniques, which include e.g., beams of fixed width and cellular coverage not exploiting beamforming. The EMF reduction is achieved not only for the UE that are served by the pencil beams, but also over the whole territory (including the locations in proximity to the 5G BS). In addition, large throughput levels - adequate for most of 5G services - can be guaranteed when each UE is individually served by one dedicated beam.

INDEX TERMS 5G cellular networks, 5G localization service, pencil beam management, EMF analysis, throughput analysis.

I. INTRODUCTION

The deployment of 5G networks is a fundamental step to provide new services that are instrumental for many sectors, including e.g., e-health, smart transportation and industry 4.0. Although the service improvements triggered by 5G technology are clear and in general well recognized, the installation of 5G next-generation Node-Bs (gNBs) over the territory generates suspect and fear among part of the population (see e.g., [1], [2]), since the Electro-Magnetic Field (EMF) exposure radiated by 5G gNBs is believed to significantly increase compared to previous generations (e.g., 2G, 3G, 4G). Not surprisingly, anti-5G movements have gained attention in recent times, claiming that 5G constitutes a danger for human health and even inspiring sabotages to destroy masts/towers hosting 5G (and pre-5G) radio equipment [3]. However, the health risks allegations that are frequently associated with 5G exposure are not confirmed by scientific evidence, especially when the levels of exposure comply with international EMF regulations [4].

In this context, the population's concerns against 5G frequently focus on the beamforming functionality [1], [5]. More specifically, a widespread opinion hypothesizes that the adoption of very narrow beams for serving the users (a.k.a. pencil beamforming) radically increases the EMF levels radiated by 5G gNBs compared to wireless stations not implementing beamforming, thus posing a serious threat for the population, and in particular for those individuals who are radiated by the traffic beams. As sketched in Fig. 1(a), the layman is firmly convinced that Base Stations (BSs) not employing pencil beamforming radiate a pretty uniform and low exposure over the territory. On the other hand, the exploitation of 5G gNBs with pencil beamforming capabilities (Fig. 1(b)) is commonly associated with an excessive EMF increase for the served users, thus fueling the population's concerns associated with 5G exposure. Despite the

The associate editor coordinating the review of this manuscript and approving it for publication was Di Zhang.

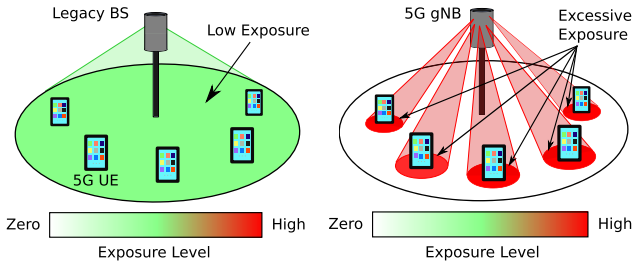

FIGURE 1. A popular layman belief: when gNBs exploiting pencil beamforming are employed (right), the level of exposure dramatically increases w.r.t. the case in which the cellular service is provided by BS not adopting beamforming (left).

research community well knows that this is not the case, as the exposure levels from 5G gNBs always comply with EMF regulations [4] - hence ensuring health safety -, to the best of our knowledge, none of the previous works investigated the exposure of pencil beamforming (Fig. 1(b)), as well as its impact when compared to other solutions (e.g, no beamforming, like in Fig. 1(a)). Therefore, the hypothesis about an EMF increase due to pencil beamforming is yet to be scientifically (and widely) refuted - even if the total exposure is still lower than the limit defined by laws.

More technically, the pencil beamforming functionality requires the localization of User Equipment (UE) that need to be served with the traffic beams. Intuitively, in fact, the knowledge of UE positioning is essential to: *i*) tune the pointing of the traffic beam(s) towards the served UE, and *ii*) adjust the width of the traffic beam in order to solely cover the area where the served UE is localized (thus avoiding unwanted exposure/interference in the neighborhood of the beam). Clearly, both *i*) and *ii*) are two fundamental steps to increase the throughput levels and consequently to match the performance levels that are required by 5G services. In this scenario, the adoption of pencil beamforming requires the integration of UE localization service in the 5G framework, a task that can be accomplished, e.g., by the LoCation Service (LCS) functionality recently introduced by 3GPP in Rel. 16 [6]. However, the exploitation of localization capabilities to manage the pencil beams and control the EMF exspoure is a relatively new and almost unexplored problem.

As a result, two fundamental questions emerge, namely: *i*) Which is the impact of pencil beamforming on the EMF exposure, especially in comparison to other solutions (e.g., no beamforming and/or traffic beams of fixed width)? *ii*) How does the uncertainty level of the UE location impact EMF and throughput levels? The goal of this paper is to provide an answer to these intriguing questions, by tackling the problem in a way that can be understood even by non-experts in the telecommunication field. More in depth, we design 5G-Pencil, a framework for the scientific evaluation of localization-enhanced pencil beamforming. 5G-Pencil implements a simple - yet effective - pencil beamforming policy that synthesizes the traffic beams by leveraging the 5G localization uncertainty level of each served user. We then code 5G-Pencil in a publicly released open source simulator, in order to evaluate both the EMF levels over the covered territory and the maximum downlink throughput achieved by each UE.

Our results, obtained over a meaningful set of case studies with realistic parameters, scientifically confute the hypothesis that pencil beamforming increases the EMF exposure. On the contrary, the localization-enhanced pencil beamforming guarantees a huge decrease of EMF exposure, which is experienced not only by the served UE but also over the whole covered territory. Moreover, the UE downlink throughput matches the 5G requirements (especially the ones for Enhanced Mobile Broadband (eMBB) scenario), even when the UE is served by one dedicated pencil beam. In addition, when the UE location is precisely estimated (with an uncertainty localization level of few meters), very narrow and almost non overlapping pencil beams are synthesized by 5G gNBs, yielding to a general exposure reduction, which is also coupled by a substantial throughput increase. Eventually, we demonstrate that the widths of the synthesized pencil beams are within meaningful ranges for 5G radio equipment.

The rest of the paper is organized as follows. Sec. II briefly reviews the related works. The main building blocks of 5G-Pencil are reported in Sec. III. Sec. IV details the localization-enhanced pencil beamforming functionality of our framework. Sec. V illustrates how 5G-Pencil is effectively implemented as an open source simulator. Results are reported in Sec. VII. Finally, Sec. VIII summarizes our work and highlights possible future avenues of research.

II. RELATED WORKS

We compare our work w.r.t. the relevant literature, by considering the following taxonomy: *i*) performance studies of beamforming in 5G networks, *ii*) health risks associated with beamforming, and *iii*) EMF assessment of beamforming.

A. PERFORMANCE OF 5G BEAMFORMING

The works belonging to this category are tailored to the assessment of throughput/capacity of cellular networks that exploit the beamforming functionality [7]–[10]. More in depth, the theoretical feasibility of beamforming as well as results from a prototype are presented in [7]. Yu *et al.* [8] propose a load balancing algorithm between macro cells and small cells, by extensively adopting a 3D beamforming feature. Awada *et al.* [9] design a channel model for signal measurement in a 5G cellular system that adopts narrow beams at fixed positions to serve the users. Ali *et al.* [10] derive closed-form expressions of the downlink Signal-to-Interference plus Noise Ratio (SINR) levels when simultaneous beams are synthesized. In contrast to [7]–[10], our work introduces a beam management policy that explicitly exploits a localization service to tune the pencil beams. In addition, we evaluate the impact of pencil beamforming not only on the throughput, but also on the EMF exposure, which represents a major concern for the population.

B. HEALTH RISKS ASSOCIATED WITH BEAMFORMING

The works falling in this category aim at finding a connection between beamforming and health risks [4], [5], [11], [12]. More in depth, according to [5], beamforming may pose an health risk, because 5G gNBs employing this feature will increase the effective radiated power. However, no scientific evidence is reported in order to support such claim. On the other hand, [11] observes that beamforming allows to transmit signals only to the served users, while the other non-users will receive a lower amount of exposure. However, a rigorous evaluation of this effect is not included. [12] reports that the adoption of beamforming may actually reduce the exposure compared to existing pre-5G technologies, without however providing any technical demonstration. Eventually, Bushberg *et al.* [4] observe that the zones that do not need to be served by active beams receive an EMF exposure sharply lower w.r.t. the ones served by legacy equipment (e.g., 4G). In contrast to [4], [5], [11], [12], our work moves three steps further by: *i*) designing a framework to technically analyze the pencil beamforming, *ii*) introducing a pencil beamforming functionality that tunes the traffic beams in accordance with the UE localization uncertainty level and *iii*) evaluating the impact of pencil beamforming on EMF and downlink throughput.

C. EMF ASSESSMENT OF BEAMFORMING

In this part, we consider the works that evaluate the EMF exposure of beamforming [13]–[18]. More specifically, Thors *et al.* [13] evaluate realistic maximum power levels of a 5G gNB employing beams focused on users. Nasim and Kim [14] evaluate the EMF exposure from 5G gNBs employing beamforming. Their model, however, assumes only fixed (and wide) beams, thus neglecting the impact of pencil beams that are oriented (and tuned) towards the single users. Basikolo *et al.* [15] show that the EMF exposure from antennas employing beamforming complies with the limits defined by international regulations. Loh *et al.* [16] focus on the experimental and statistical assessment of the EMF exposure from 5G gNBs in indoor environments, by considering beams oriented towards the UE. Xu *et al.* [17] show that simple models can be employed to determine the exclusion zones from gNBs operating with Multiple-Input Multiple-Output (MIMO) and beamforming features. Adda *et al.* [18] observe that only a fraction of the total gNB power is radiated towards each single user, thus leading to a decrease of the EMF levels. In contrast to [13]–[18], we introduce the following key novelties: *i*) we design a framework that is able to synthesize the pencil beams in accordance with the UE localization uncertainty level (a feature not exploited at all by previous works), and *ii*) we demonstrate that the decrease of UE localization uncertainty level can further reduce the EMF generated by pencil beamforming.

III. 5G-PENCIL FRAMEWORK: BUILDING BLOCKS

Fig. 2 reports the high-level view of the main building blocks that compose the 5G-Pencil framework and their interaction with a set of core functionalities of the 5G architecture

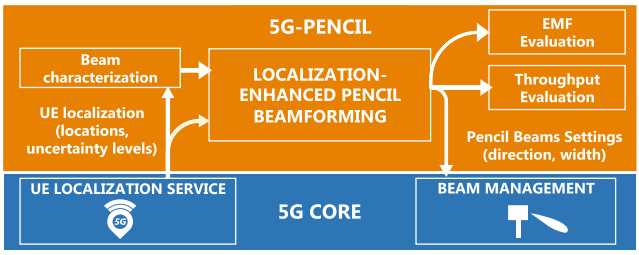

FIGURE 2. 5G-Pencil framework: building blocks and interactions with the features implemented in the core of 5G architecture.

(i.e., external to our framework). More in depth, for each 5G user for which a localization service is available, an estimation of the UE location and an associated uncertainty level is provided by the 5G core. Such information is then exploited by 5G-Pencil to characterize the main features of each beam that needs to be synthesized, including e.g., selection of the coordinate system and computation of the pointing angles. The central part of the framework is the localization-enhanced pencil beamforming module, which computes the beam pointing and the beam width to serve each UE, based on UE localization as well as the information generated by the beam characterization module. This is a key innovative contribution of our work: when localization information is exploited to tune the beams, it is possible e.g., to synthesize narrow pencil beams towards the UE that are localized with a given accuracy level. Moreover, 5G-PENCIL includes: *i*) the EMF evaluation module, which computes the exposure that is generated by the synthesized beams over the territory; and *ii*) the throughput evaluation module to compute the downlink performance for each UE. Finally, the pencil beam settings are passed to the 5G core for the beam management functionality, which implements the set of beams in the deployed 5G network.

In the rest of the section, we provide more details about the following modules: *a*) UE localization, *b*) beam characterization, *c*) EMF evaluation, *d*) throughput evaluation and *e*) beam management. We intentionally leave apart the innovative localization-enhanced pencil beamforming, which is detailed in Sec. IV. In addition, we stress the fact that our paper is the first work to integrate together *a*)-*e*) in an unique framework, which is instrumental for the localization-enhanced pencil beamforming and consequently for the goal of assessing the impact of pencil beamforming in terms of exposure (and throughput).

A. USER EQUIPMENT LOCALIZATION

5G UE localization is introduced in Rel. 15 of 3GPP, through the definition of the location management function within 5G positioning [6]. The UE location is computed from measurements mainly based on DownLink Time Difference of Arrival (DL-TDoA) and beamforming Angle of Arrival (AoA) between the gNBs and the UE. Position accuracy is defined by 3GPP as the difference between actual location and estimated location and it is thus related to the uncertainty level of the UE position. More specifically, the UE location

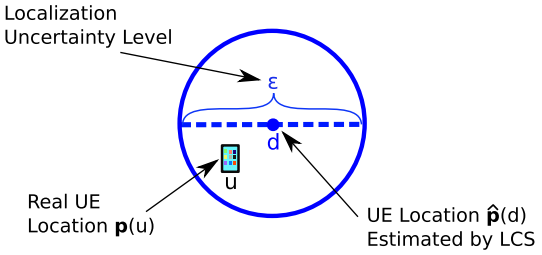

FIGURE 3. Comparison among real UE location $\mathbf{p}(u)$ and UE location $\hat{\mathbf{p}}(d)$ estimated by LCS. The figure reports also the uncertainty level for the estimated UE location as a circle of diameter ϵ.

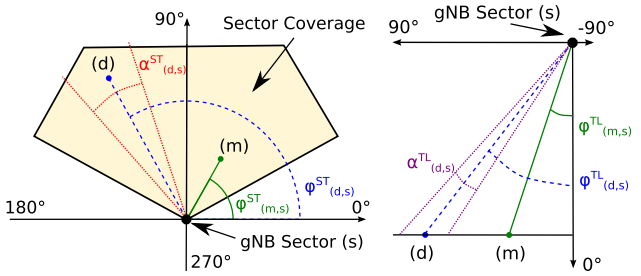

FIGURE 4. Definition of the angles for a toy case scenario with a sector coverage equal to 1/3 of an hexagon, one beam deployed over d from s and one measurement spot m.

uncertainty level varies across the network geographic area depending on the UE true position, due to a multitude of factors, which include, e.g., variability of radio conditions, cell configuration and cell density. In addition, the accuracy can be negotiated based on the requirements of the specific 5G service that needs to be provided. According to the 3GPP technical specifications in Rel. 16 [19], the LCS shall satisfy or approach as closely as possible the requested or negotiated accuracy when other Quality of Service (QoS) parameters are not in conflict.

More formally, the achieved accuracy level of location information is expressed through the shapes and the uncertainty areas defined in [20]. An uncertainty circle indicates a point when its position is known only with a limited accuracy, with an uncertainty level that is described by the circle diameter.[1] To this aim, Fig. 3 reports a representative example in which $\hat{\mathbf{p}}(d)$ denotes the estimated UE position, which is defined as an integer index d to extract a row of x-y-z coordinates from array $\hat{\mathbf{p}}$. The circle of diameter ϵ is the localization uncertainty area in the horizontal plane. Finally, $\mathbf{p}(u)$ is the real UE location, which is expressed as integer index u to extract a row of x-y-z coordinates from array $\mathbf{p}$. For the sake of simplicity, we get rid of coordinates arrays $\mathbf{p}$ and $\hat{\mathbf{p}}$ from now on, by simply referencing to the real (estimated) UE location through index u (d).

In our context, the UE localization is provided by the LCS functionality implemented in the 5G network. As a result, 5G-Pencil takes as input the estimated location d for each UE, together with the uncertainty level ϵ.

B. BEAM CHARACTERIZATION

Let us consider a generic sector s of 5G gNB and two points d and m located in the territory. Point d is the estimated UE location already introduced in Fig. 3. Such position is assumed to be the target of a deployed beam, and therefore it is referred hereafter as "deployment spot". On the other hand, m is named "measurement spot", because such location is used to evaluate EMF that is generated by the beam targeting d. Let us then assume two observation planes for the sector, one horizontal (i.e., azimuth) and one vertical (i.e., elevation). Focusing on the horizontal plane, we introduce an angular orientation system centered on s, spanning from 0° to 360°, as shown in Fig. 4(a). Let us denote with $\phi^{\mathrm{ST}}_{(d,s)}$ the steering angle of d w.r.t. sector s. In a similar way, $\phi^{\mathrm{ST}}_{(m,s)}$ is the steering angle that is measured over m from s. Focusing then on the vertical plane, we introduce an angular orientation system between 90° and -90°, again centered on s, as shown in Fig. 4(b). We then denote as $\phi^{\mathrm{TL}}_{(d,s)}$ and $\phi^{\mathrm{TL}}_{(m,s)}$ the tilting angles of d and m w.r.t. sector s respectively.

In the following, we introduce the notation to characterize the beam widths. Specifically, we adopt the commonly-used assumption that the width is denoted by the cone where the beam gain is at most 3 [dB] lower than the maximum value (i.e., the one achieved over $\phi^{\mathrm{ST}}_{(d,s)}$ and $\phi^{\mathrm{TL}}_{(d,s)}$). More in depth, let us denote with $\alpha^{\mathrm{ST}}_{(d,s)}$ the projection on the horizontal plane of the 3 [dB] beam cone used to serve deployment spot d from s. Similarly, let us denote with $\alpha^{\mathrm{TL}}_{(d,s)}$ the projection of the same 3 [dB] beam cone on the vertical plane. As shown in Fig. 4, both $\alpha^{\mathrm{ST}}_{(d,s)}$ and $\alpha^{\mathrm{TL}}_{(d,s)}$ are expressed as relative angles, and therefore they do not depend on the absolute angular positioning systems adopted for s. Intuitively, the setting of $\alpha^{\mathrm{ST}}_{(d,s)}$ and $\alpha^{\mathrm{TL}}_{(d,s)}$ heavily influences the size of the area covered by the beam, which in turns affects both throughput and EMF values. Consequently, the optimization of $\alpha^{\mathrm{ST}}_{(d,s)}$ and $\alpha^{\mathrm{TL}}_{(d,s)}$ values is one of the key goals that are targeted by our framework.

To summarize, the beam that covers deployment spot d from s is fully denoted by the quadruple $\phi^{\mathrm{ST}}_{(d,s)}$, $\phi^{\mathrm{TL}}_{(d,s)}$, $\alpha^{\mathrm{ST}}_{(d,s)}$, $\alpha^{\mathrm{TL}}_{(d,s)}$. In addition, each measurement spot m is characterized by angles $\phi^{\mathrm{ST}}_{(m,s)}$ and $\phi^{\mathrm{TL}}_{(m,s)}$.

C. EMF EVALUATION

Let us assume that a pencil beam is deployed over d by a radiating element installed on s, and that we want to compute the exposure generated by this beam over m. In line with International Telecommunication Union (ITU) recommendations [21], [22], as well as previous works [23], we assume an exclusion zone - whose access is prohibited to the general public - in proximity to the gNB. Since our goal is to evaluate the impact of pencil beamforming on the population (i.e., not for maintenance workers who may sporadically operate inside the gNB exclusion zone), both m and d are outside the exclusion zone of s. Consequently, the EMF is

[1] Alternatively, the uncertainty level can be expressed as the circle radius. In this work, however, we stick to the assumption that the uncertainty level corresponds to the circle diameter.

always evaluated in the far-field region, where the exposure is expressed in terms of EMF strength and/or Power Density (PD) [21], [22].[2] This choice is also supported by the fact that the exposure limits from gNBs are normally defined as maximum EMF strength (or, equivalently, as maximum PD) [24]. In addition, the on-the-field measurement of the exposure levels from gNBs is typically performed by employing meters that measure EMF strength [22].

More formally, we start from the widely-accepted point-source model of ITU [21] to compute the PD $S_{(d,s,m)}$ that is received by m from the pencil beam serving d from s:[3]

$$S_{(d,s,m)} = \frac{P_s^{\text{EIRP}} \cdot F_{(d,s,m)}}{4\pi \cdot \delta_{(s,m)}^2} \tag{1}$$

where P_s^{EIRP} is the Equivalent Isotropically Radiated Power (EIRP) of the antenna element installed on sector s, $F_{(d,s,m)} \in (0, 1]$ is the antenna numeric gain observed over m w.r.t. the pencil beam serving d from s, and $\delta_{(s,m)}$ is the 3D distance between s and m.

The term P_s^{EIRP} is then expressed as:

$$P_s^{\text{EIRP}} = P_s^{\text{MAX}} \cdot G^{\text{MAX}} \tag{2}$$

where P_s^{MAX} is the maximum radiated power by one antenna element on sector s and G^{MAX} is the maximum antenna gain.

Focusing instead on $F_{(d,s,m)}$, we express the normalized numeric gain as in [21]:

$$F_{(d,s,m)} = \left(10^{\frac{A_{(d,s,m)}^{\text{AZ}} + A_{(d,s,m)}^{\text{EL}}}{10}}\right)^2 \tag{3}$$

where $A_{(d,s,m)}^{\text{AZ}}$ and $A_{(d,s,m)}^{\text{EL}}$ are the azimuth and the elevation radiation patterns (in [dB]) observed over m from an antenna element in sector s serving deployment spot d.

Both $A_{(d,s,m)}^{\text{AZ}}$ and $A_{(d,s,m)}^{\text{EL}}$ are then expressed as in [8], by adopting the angles already introduced to characterize the beam over d and the measurement spot m:

$$A_{(d,s,m)}^{\text{AZ}} = -\min\left[12\left(\frac{\phi_{(m,s)}^{\text{ST}} - \phi_{(d,s)}^{\text{ST}}}{\alpha_{(d,s)}^{\text{ST}}}\right)^2, A_{\text{MIN}}^{\text{AZ}}\right] \tag{4}$$

$$A_{(d,s,m)}^{\text{EL}} = -\min\left[12\left(\frac{\phi_{(m,s)}^{\text{TL}} - \phi_{(d,s)}^{\text{TL}}}{\alpha_{(d,s)}^{\text{TL}}}\right)^2, A_{\text{MIN}}^{\text{EL}}\right] \tag{5}$$

where $A_{\text{MIN}}^{\text{AZ}}$ and $A_{\text{MIN}}^{\text{EL}}$ are the front-to-back ratio and the side lobe level limit, respectively. By analyzing in detail Eq. (4), we can note that the maximum radiation patterns are achieved when $\phi_{(m,s)}^{\text{ST}} = \phi_{(d,s)}^{\text{ST}}$ and $\phi_{(m,s)}^{\text{TL}} = \phi_{(d,s)}^{\text{TL}}$, i.e., the measurement spot m is co-located with d. In addition, the beam widths α_s^{ST} and α_s^{TL} act as scaling parameters for the radiation pattern: the higher is the beam width, the lower is the impact of the steering/tilting angles and consequently the larger is the radiation pattern. Finally, the front-to-back ratio and the side lobe level limit are used to bound the minimum radiation pattern values.

In the following, we extend the exposure model by considering a set of deployment spots $\mathcal{D}$ and a set of gNB sectors $\mathcal{S}$. To this aim, let us introduce parameter $X_{(d,s)}$, taking value 1 if $d \in \mathcal{D}$ is served by $s \in \mathcal{S}$, 0 otherwise. The overall exposure over measurement point m by all the beams that are deployed in the scenario is then expressed as:

$$S_m^{\text{TOT}} = \sum_{s \in \mathcal{S}} \sum_{d \in \mathcal{D}} S_{(d,s,m)} \cdot X_{(d,s)} \tag{6}$$

Finally, we exploit the widely-known equivalence between EMF strength and PD [21] (which we remind is valid in the far-field region) to compute the total EMF strength observed in m:

$$E_m^{\text{TOT}} = \sqrt{S_m^{\text{TOT}} \cdot Z} \tag{7}$$

where $Z = 377$ [Ω] is the free-space wave impedance.

Two considerations hold by analyzing Eq. (1)-(7). First, the total exposure generated by multiple beams deployed in the scenario is evaluated for each measurement spot $m \in \mathcal{M}$. Second, the point-source model of Eq. (1) is an upper bound of the actual level of exposure that is measured on-the-field [21], thus substantiating the outcomes of our work.

D. THROUGHPUT EVALUATION

We initially evaluate the throughput that is received by a generic user located at position u inside deployment spot d. For simplicity, we assume that deployment spot d is served by one single dedicated beam that is radiated by sector s. The maximum downlink throughput $T_{(d,s,u)}$ is computed with the classical Shannon capacity model:

$$T_{(d,s,u)} = B_s \cdot \log_2(1 + \text{SINR}_{(d,s,u)}) \tag{8}$$

where B_s is the adopted bandwidth and $\text{SINR}_{(d,s,u)}$ is the SINR experienced at u, due to the beam that is deployed over d from s.

We then express the SINR as the one used by the multiple-beam system [10]:

$$\text{SINR}_{(d,s,u)} = \frac{P_{(d,s,u)}^{\text{RX}}}{\underbrace{\sum_{d' \neq d} P_{(d',s,u)}^{\text{RX}}}_{\text{Intra-sector Interference}} + \underbrace{\sum_{d' \neq d} \sum_{s' \neq s} P_{(d',s',u)}^{\text{RX}}}_{\text{Inter-sector Interference}} + N} \tag{9}$$

where $P_{(d,s,u)}^{\text{RX}}$ is the power received at u from the beam deployed over d by s and N is the noise component. From Eq. (9), we can note that each beam can interfere with all the others that are deployed from the same sector (intra-sector term) and/or from other sectors (inter-sector term). In order to

[2] An alternative metric to characterize the exposure is the Specific Absorption Rate (SAR), which is usually employed to evaluate the exposure levels in near-field regions, especially for personal devices operating in close proximity to the body, like smartphones. Since our goal is to evaluate the level of exposure from gNBs in the far-field region, the evaluation of exposure in terms of EMF strength / PD provides a more meaningful information than SAR.

[3] The suitability of using the point-source model for evaluating the exposure of gNBs employing beamforming is also confirmed by [17].

evaluate the throughput under different interference assumptions, in this work we consider the computation of the SINR with and without intra-sector interference. Clearly, when the intra-sector term is not considered, the throughput tends to be higher, because the beams generated by the same sector do not interfere with each other.

In line with [10], we express the received power $P^{RX}_{(d,s,u)}$ (in [dB]) as:

$$P^{RX}_{(d,s,u)} = \underbrace{P^{TX}_{s}}_{\text{Max. Tx Power}} - \underbrace{L^{PL}_{(s,u)}}_{\text{3D Path Loss}} + \underbrace{A^{AZ}_{(d,s,u)} + A^{EL}_{(d,s,u)}}_{\text{Beam radiation pattern}} + \underbrace{G^{TX}_{s}}_{\text{Max. Tx Gain}} + \underbrace{B^{AZ}_{(d,s,u)} + B^{EL}_{(d,s,u)} + G^{BF}_{s}}_{\text{Beamforming gain}} \quad (10)$$

where P^{TX}_{s} is the maximum transmission power of the entire antenna array located at s, $L^{PL}_{(s,u)}$ is the 3D path loss term between s and u, $A^{AZ}_{(d,s,u)}$ and $A^{EL}_{(d,s,u)}$ are the antenna radiation patterns already defined in Eq. (4),(5) (computed here w.r.t. UE location u), G^{TX}_{s} is the maximum transmission gain of one antenna element in s, G^{BF}_{s} is the maximum beamforming gain for s, while the beamforming terms $B^{AZ}_{(d,s,u)}$ and $B^{EL}_{(d,s,u)}$ are formally expressed as in [9]:

$$B^{AZ}_{(d,s,u)} = 10\log_{10}\left[\text{sinc}\left(\frac{\phi^{ST}_{(u,s)} - \phi^{ST}_{(d,s)}}{1.13 \cdot \alpha^{ST}_{(d,s)}}\right)^2\right] \quad (11)$$

$$B^{EL}_{(d,s,u)} = 10\log_{10}\left[\text{sinc}\left(\frac{\phi^{TL}_{(u,s)} - \phi^{TL}_{(d,s)}}{1.13 \cdot \alpha^{TL}_{(d,s)}}\right)^2\right] \quad (12)$$

By analyzing in detail Eq. (10)-(12), we can note that the received power is computed as a combination of different terms that scale the maximum transmission power of the entire antenna array. As a result, the level of detail provided by the throughput model is higher compared to the EMF one. However, also in this case the beam widths severely impact both the beam radiation patterns and the beamforming gain terms, thus affecting the received power and hence in turn the received throughput.

E. BEAM MANAGEMENT

The set of traffic beams that are selected by our framework is then passed as input to the beam management module of the 5G network. Apart from synthesizing the pencil beams on the deployed gNBs, this module controls the set of beam(s) that are deployed to provide basic coverage (a.k.a. "broadcast beams") and/or for retrieving the UE localization information. However, the exposure from such additional beams is overall much lower than the EMF radiated by the traffic beams, as shown e.g., in [18]. Therefore, the EMF evaluation in our framework is intentionally focused on the impact of traffic beams in terms of EMF (and throughput).

IV. LOCALIZATION-ENHANCED PENCIL BEAMFORMING

We initially introduce a set of simplifying and/or conservative assumptions that are instrumental for the pencil beamforming module. Then, we detail the algorithm that we have designed to tune the pencil beams on the deployment spots.

A. MAIN ASSUMPTIONS

We consider the adoption of antenna arrays composed of a large number of radiating elements, denoted as N^{R}_{s}. Each gNB hosts a set of non-overlapping sectors, each of them equipped with an antenna array. Each radiating element is able to generate a traffic beam that is characterized by a given direction and by a given width in the area covered by the sector. We then assume that each deployment spot $d \in \mathcal{D}$ is served by at most one dedicated pencil beam. Although this assumption may appear relatively conservative at a first glance, as d may be alternatively served by multiple pencil beams at the same time, we demonstrate that the throughput level achieved with one pencil beam over d already matches the performance level required by 5G, thus substantiating our analysis.[4] Moreover, we assume that the number of radiating elements N^{R}_{s} is always higher or equal than the number of deployment spots placed in each sector. In this way, all the UE in the territory are served by our framework.

Finally, we introduce a set of assumptions for the pencil beams. More precisely: *i)* the pencil beams are activated all together at the same time, and *ii)* each pencil beam always transmits at the maximum power in the downlink direction, i.e., no traffic adaptation mechanisms are applied to the power radiated by the beam. In this way, we evaluate EMF (throughput) under high exposure (peak traffic) conditions.

B. ALGORITHM DESCRIPTION

Alg. 1 reports the high-level pseudocode of the pencil beam setting procedure implemented in 5G-Pencil. The algorithm requires as input the set of sectors $\mathcal{S}$, the set of deployment spots $\mathcal{D}$ and the localization uncertainty level ϵ (which are passed to 5G-Pencil by the UE localization service module), as well as the minimum values for the beam width in the horizontal and vertical planes, denoted as α^{ST}_{MIN} and α^{TL}_{MIN}, respectively. Intuitively, in fact, the minimum beam widths are constrained by the technological features of the antenna arrays, which can synthesize pencil beam of a given width up to minimum values α^{ST}_{MIN} and α^{TL}_{MIN}. The algorithm then returns as output the deployment spot-sector association array $X_{(d,s)}$, as well as the selected pencil width settings $\alpha^{ST}_{(d,s)}$ and $\alpha^{TL}_{(d,s)}$.

Initially, (lines 3-4), the algorithm iterates over the elements in $\mathcal{S}$ and in $\mathcal{D}$. For each pair (d, s), a coverage check is performed. This function is intentionally not expanded Alg. 1, due to the fact that the (d, s) association is a choice left to the operator, which may associate a deployment spot to a sector depending on multiple factors, including, e.g., link budget evaluation at the UE location, maximum coverage distance between s and d, traffic load distribution among the gNBs and/or a mixture between them. If d can be covered by s, then

[4]The investigation of multiple pencil beams serving each UE is left for future work.

Algorithm 1 Localization-Enhanced Pencil Beam Tuning

1: **Input:** $\mathcal{S}$, $\mathcal{D}$, ϵ, $\alpha^{\mathrm{ST}}_{\mathrm{MIN}}$, $\alpha^{\mathrm{TL}}_{\mathrm{MIN}}$
2: **Output:** $X_{(d,s)}$, $\alpha^{\mathrm{ST}}_{(d,s)}$, $\alpha^{\mathrm{TL}}_{(d,s)}$
3: **for** s in $\mathcal{S}$ **do**
4: **for** d in $\mathcal{D}$ **do**
5: **if** check_coverage(d,s) == true **then**
6: *// Deployment spot - sector association*
7: $X_{(d,s)} = 1$;
8: *// Interception points computation*
9: $[I^{\mathrm{W}}_{(d,s)}, I^{\mathrm{E}}_{(d,s)}, I^{\mathrm{N}}_{(d,s)}, I^{\mathrm{S}}_{(d,s)}]$ = comp_pt(d,s,ϵ);
10: *//Horizontal width setting*
11: $\lambda^{\mathrm{H}}_{c} = I^{\mathrm{W}}_{(d,s)} \overset{\mathrm{H}}{\rightarrow} (s)$;
12: $\lambda^{\mathrm{H}}_{b} = \lambda^{\mathrm{H}}_{a}$;
13: $\lambda^{\mathrm{H}}_{a} = I^{\mathrm{W}}_{(d,s)} \overset{\mathrm{H}}{\rightarrow} I^{E}_{(d,s)}$;
14: tmp_angle_st $= \arccos\left(1 - \frac{(\lambda^{\mathrm{H}}_{a})^2}{2\cdot(\lambda^{\mathrm{H}}_{c})^2}\right)$;
15: $\alpha^{\mathrm{ST}}_{(d,s)} = \max(\text{tmp\_angle\_st}, \alpha^{\mathrm{ST}}_{\mathrm{MIN}})$;
16: *//Vertical width setting*
17: $\lambda^{\mathrm{V}}_{c} = I^{\mathrm{N}}_{(d,s)} \overset{\mathrm{V}}{\rightarrow} (s)$;
18: $\lambda^{\mathrm{V}}_{b} = I^{\mathrm{S}}_{(d,s)} \overset{\mathrm{V}}{\rightarrow} (s)$;
19: tmp_angle_tl $= \arccos\left(\frac{(\lambda^{\mathrm{V}}_{c})^2+(\lambda^{\mathrm{V}}_{b})^2-\epsilon^2}{2\cdot\lambda^{\mathrm{V}}_{c}\cdot\lambda^{\mathrm{V}}_{b}}\right)$;
20: $\alpha^{\mathrm{TL}}_{(d,s)} = \max(\text{tmp\_angle\_tl}, \alpha^{\mathrm{TL}}_{\mathrm{MIN}})$;
21: **end if**
22: **end for**
23: **end for**

the serving variable $X_{(d,s)}$ is set to 1 (line 7) and a pencil beam is tuned on d from s (lines 8-20).

In order to better explain the further steps of the beam setting procedure, Fig. 5 reports a graphical sketch including one sector s and one deployment spot d, subject to an uncertainty localization level equal to ϵ. Let us consider two lines T^{E} and T^{W} passing from the projection of s on the horizontal plane and tangent to the deployment spot shape (i.e., the circle centered in d of diameter ϵ). The interception point between T^{E} (T^{W}) and the circle is denoted as $I^{\mathrm{E}}_{(d,s)}$ ($I^{\mathrm{W}}_{(d,s)}$). The angle centered on the projection of s on the horizontal plane and spanning between $I^{\mathrm{E}}_{(d,s)}$ and $I^{\mathrm{W}}_{(d,s)}$ represents $\alpha^{\mathrm{ST}}_{(d,s)}$. Let us now consider a straight line T^{C} starting from the projection of s on the horizontal plane and passing through d. The interception points between T^{C} and the circular area delimiting the deployment spot are then denoted with $I^{\mathrm{N}}_{(d,s)}$ and $I^{\mathrm{S}}_{(d,s)}$, respectively. The angle centered in s on the vertical plane and spanning between $I^{\mathrm{N}}_{(d,s)}$ and $I^{\mathrm{S}}_{(d,s)}$ denotes $\alpha^{\mathrm{TL}}_{(d,s)}$.

Up to this point, a natural question is then: How to compute $\alpha^{\mathrm{ST}}_{(d,s)}$ and $\alpha^{\mathrm{TL}}_{(d,s)}$? To answer this question, we preliminary identify the triangle of edges $I^{\mathrm{W}}_{(d,s)} \overset{\mathrm{H}}{\rightarrow} (s) \overset{\mathrm{H}}{\rightarrow} I^{\mathrm{E}}_{(d,s)} \overset{\mathrm{H}}{\rightarrow} I^{\mathrm{W}}_{(d,s)}$, where the $(\cdot) \overset{\mathrm{H}}{\rightarrow} (\cdot)$ notation denotes the two endpoints of the edge on the horizontal plane. In a similar way, we identify on the vertical plane the triangle of edges $I^{\mathrm{N}}_{(d,s)} \overset{\mathrm{V}}{\rightarrow} (s)$, $I^{\mathrm{S}}_{(d,s)} \overset{\mathrm{V}}{\rightarrow} (s)$ and ϵ. Given the triangle edges, we then apply the law of cosines (a.k.a. al-Kashi's theorem or Carnot's theorem) to compute $\alpha^{\mathrm{ST}}_{(d,s)}$ and $\alpha^{\mathrm{TL}}_{(d,s)}$, as detailed in lines (10-20) of Alg. 1. Clearly, the algorithm ends when all the pairs (d, s) have been analyzed.

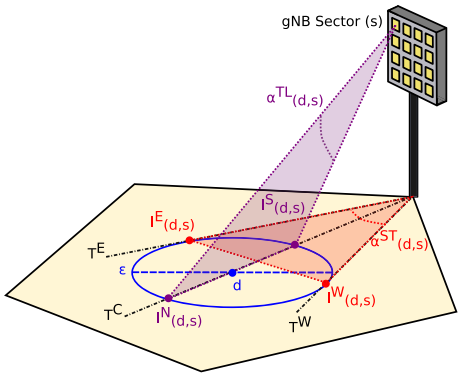

FIGURE 5. Graphical sketch of the interception points and the triangles that are used to tune the pencil width.

Focusing on Alg. 1, the beam width is scaled in accordance with the position of d and with the uncertainty localization level ϵ. Intuitively, when a deployment spot is close to the serving gNBs, the beam width will be higher than the one of the spots located at the sector edge. In a similar way, the beam width is decreased when the localization uncertainty level is reduced, thus allowing the synthesis of narrower pencil beams.

V. 5G-Pencil IMPLEMENTATION

We code 5G-Pencil as an open-source simulator, which is publicly available for download [25]. Fig. 6 reports the block diagram of our implementation. During step S1, the simulator generates a candidate set of gNBs from a given coverage tessellation and a given number of sectors for each gNB. This phase also includes the definition of the exclusion zone for each gNB. During step S2, we generate the deployment spots, the real UE locations, and the measurement spots. The number of deployment spots per sector is an input parameter, bounded to N^{R}_{s}, i.e., the number of radiating elements of each antenna array. The spatial positioning of deployment spots on the horizontal plane integrates multiple options, which include, e.g., an uniform positioning across the sector extent or a preferential generation of the spots in proximity of the sector (in order to mimic a hot-spot zone). For each deployment spot d, we randomly generate the real UE location as a point inside the circle of diameter ϵ, centered in d. Focusing then on the measurement spots, an uniform grid of equally spaced deterministic points is assumed over the whole covered territory (except inside the gNBs exclusion zone). During step S3, the simulator computes the angles $\phi^{\mathrm{ST}}_{(d,s)}$, $\phi^{\mathrm{TL}}_{(d,s)}$, $\phi^{\mathrm{ST}}_{(m,s)}$, $\phi^{\mathrm{TL}}_{(m,s)}$, $\phi^{\mathrm{ST}}_{(u,s)}$, $\phi^{\mathrm{TL}}_{(u,s)}$, for each deployment spot $d \in \mathcal{D}$, each measurement spot $m \in \mathcal{M}$, each real UE location, and each sector $s \in \mathcal{S}$. In the following step (S4), the localization-enhanced pencil beamforming algorithm is executed. Consequently, both the variable $X_{(d,s)}$ and the beam widths $\alpha^{\mathrm{ST}}_{(d,s)}$ and $\alpha^{\mathrm{TL}}_{(d,s)}$ are set. During S5-S6, the throughput

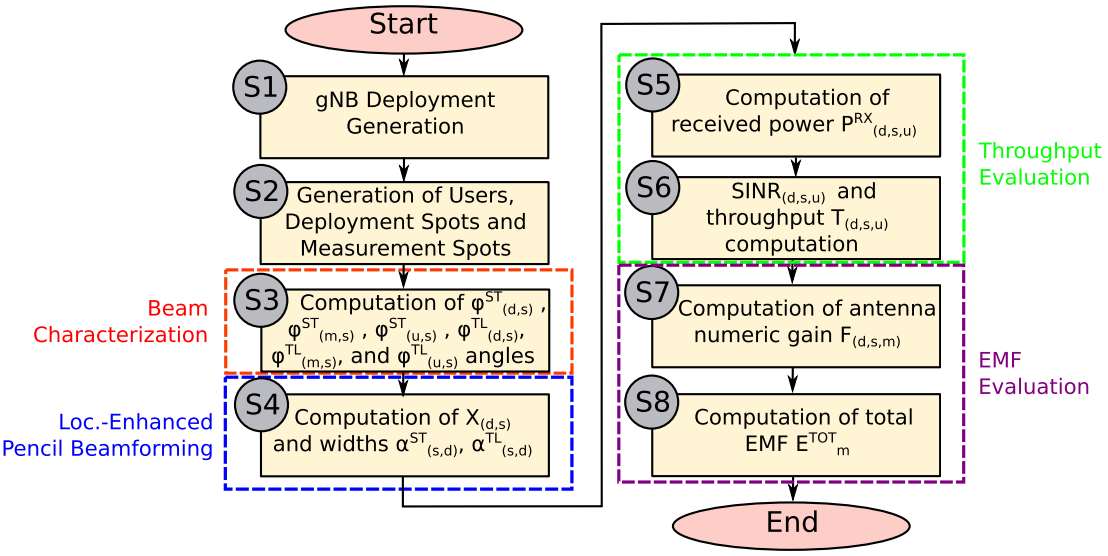

FIGURE 6. Block diagram of the 5G-Pencil implementation.

is evaluated, by adopting the model detailed in Sec. III-D. Finally, the EMF of the pencil beam is computed in S7-S8, by adopting the procedure described in Sec. III-C.

VI. SCENARIO DESCRIPTION

We consider a simple, yet meaningful scenario, to evaluate the impact of pencil beamforming that is achieved by running the 5G-Pencil framework. To this aim, Tab. 1 reports the settings for the main input parameters. More specifically, we consider a regular cellular deployment, where a set of $N^{\text{gNB}} = 7$ gNBs are placed on an hexagonal grid. We then assume that the coverage area of each gNB is an hexagon of side $L = 100$ [m], thus matching an urban/dense urban 5G deployment. Moreover, each gNB is equipped with $N^{\text{SEC}} = 3$ non-overlapping sectors, with a circular exclusion zone of radius $R_s^{\text{MIN}} = 10$ [m] around the gNB location (set in accordance with [23]). The total number of sectors $|\mathcal{S}|$ is then equal to $N^{\text{gNB}} \cdot N^{\text{SEC}} = 21$. Each sector is equipped with $N_s^{\text{R}} = 64$ radiating elements, as reported by relevant datasheets of 5G equipment [26]. Focusing then on the deployment spots generation, we assume that each sector simultaneously serves the maximum number of spots, which corresponds to $N_s^{\text{R}} = 64$. Consequently, the total number of deployment spots over all the sectors is equal to $|\mathcal{S}| \cdot N_s^{\text{R}} = 448$. The set of deployment spots in each sector is generated by randomly picking polar coordinates over the sector extent, which then results in a set of spots preferentially generated in the surroundings of the sector center. Finally, Fig. 7 a graphical sketch of the considered set of sectors, as well as one exemplary generation of deployment spots.

In the following, we move our attention on the selection of the zones in which the EMF and the throughput are evaluated. Focusing on the former, we deploy an uniform grid of squared measurement spots with resolution of 1 [m] × 1 [m], covering the area of the central gNB (outside the gNB exclusion zone). In this way, each measurement spot receives exposure

TABLE 1. Settings of the Main Input Parameters.

Symbol	Description	Value/Reference
-	gNB Deployment	Hexagonal grid
N^{gNB}	Number of gNBs	7
N^{SEC}	Number of sectors per gNB	3 (with 120° orientation)
L	Sector side	100 m
N_s^{R}	Number of radiating elements per sector	64 [26]
$\|\mathcal{S}\|$	Total number of sectors	$N^{\text{gNB}} \cdot N^{\text{SEC}} = 21$
$\|\mathcal{D}\|$	Number of deployment spots	$\|\mathcal{S}\| \cdot N_s^{\text{R}} = 448$
-	Deployment spot positioning	Hot-spot placement with random polar coordinates
-	Coverage check	Based on Voronoi region (with sectorization)
$\|\mathcal{U}\|$	Number of real UE locations	$N^{\text{SEC}} \cdot N_s^{\text{R}} = 192$ (central gNB)
-	Real UE location positioning	Random placement based on Cartesian coordinates in the circle centered in d with radius ϵ
$\|\mathcal{M}\|$	Number of measurement spots	25572 (central gNB with 1 m × 1 m resolution)
R_s^{MIN}	Exclusion Zone Radius	10 m [23]
P_s^{TX}	Max. TX power per antenna array	200 W [23]
P_s^{MAX}	Power of one antenna element	$P_s^{\text{TX}}/N_s^{\text{R}} = 3.125$ W (Uniform power splitting among the antenna elements)
G^{MAX}	Maximum antenna gain	15 dBi [26]
$A_{\text{MIN}}^{\text{AZ}}$	Front-to-back ratio	25 dB [8]
$A_{\text{MIN}}^{\text{EL}}$	Side lobe limit	20 dB [8]
B_s	Sector bandwidth	80 MHz [27]
F_s	Sector operating frequency	3.7 GHz [27]
H_s	Sector height above ground	15 [m]
H_d H_m H_u	Deployment spot/measurement spot/UE height above ground	1.5 [m]
$L_{(s,u)}^{\text{PL}}$	3D path loss between s and u	3GPP UMi-Street Canyon LOS/NLOS models [28]
G_s^{TX}	TX gain per antenna element	3 dBi [9]
G_s^{BF}	Maximum beamforming gain	$10 \cdot \log_{10}(N_s^{\text{R}})$ [9]
N_s	Noise term	Noise power from [29] with 5 dB noise figure and B_s bandwidth
$\alpha_{\text{MIN}}^{\text{ST}}$	Minimum width angle (steering)	3°
$\alpha_{\text{MIN}}^{\text{TL}}$	Minimum width angle (tilting)	3°
ϵ	Uncertainty localization level	$\{20, 16, 8, 4, 2\}$ m (Range covering PSL 1-6 [30])

from both the serving sector as well as the neighboring ones (from other gNBs), while limiting the border effects that may emerge in the outer sectors. Consequently, the EMF is evaluated over more than 25000 measurement spots. In a

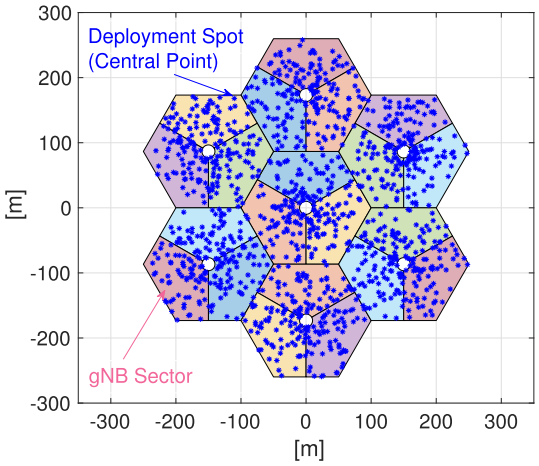

FIGURE 7. Example of gNBs and deployment spots positioning in 5GPencil.

similar way, we restrict the throughput evaluation only for the area covered by the central gNB. In this area, we randomly generate each UE location within the circle centered in d (corresponding to the estimated UE location), with radius ϵ. Consequently, the throughput is evaluated over more than 190 UE locations.

We then focus on the parameters that are needed by the EMF and throughput models. We refer the reader to Tab. 1 for the detailed explanation of each parameter setting, while here we discuss the salient features. In brief, most of parameters are taken from the literature, product datasheets and/or real deployment options. Focusing on the bandwidth and frequency, we consider the deployment of gNBs operating in the mid-band (i.e., 3.7 [GHz] of operating frequency), with 80 [MHz] of available bandwidth for each sector.[5] In addition, we assume that the total power consumption of the antenna array is uniformly split across the radiating elements. Consequently, the power of one antenna element P_s^{MAX} is set equal to 3.125 [W]. As an additional comment, we consider the 3GPP UMi-Street Canyon propagation model [28] under both Line-of-Sight (LOS) and Non-Line of Sight (NLOS) conditions. To this aim, each gNB sector is placed at height of 15 [m] above ground level (corresponding to a pole-mounted and/or roof-top installation), while the EMF and the throughput are evaluated at an height of 1.5 [m] above ground level.

Focusing then on the technology constraints to synthesize the beams, we have to select the minimum beam widths $\alpha_{\text{MIN}}^{\text{ST}}$ and $\alpha_{\text{MIN}}^{\text{TL}}$. Although the exact settings of such parameters is strongly influenced by the adopted beamforming architecture (see e.g., [31]), in this work we consider $\alpha_{\text{MIN}}^{\text{ST}} = \alpha_{\text{MIN}}^{\text{TL}} = 3°$, due to the following reasons. First, such setting is in line with other relevant works targeting beam management in 5G networks (see e.g., [32]). Second, it is expected that 5G gNB adopting pencil beamforming will be able to synthesize very narrow traffic beams (i.e., in the order of few degrees).

Finally, we take into account the setting for one of the most impacting parameters: the localization uncertainty level ϵ. To this aim, we rely on Positioning Service Level (PSL) 1-6 defined in [30], which correspond to the accuracy requirements that 5G networks should fulfill according to the 3GPP definition of location services.[6] Intuitively, each PSL is characterized by given values of horizontal/vertical accuracy and absolute/vertical position, by considering other timing Key Performance Indicators (KPIs), as well as by taking into account the different operating environments and network coverage. Tab. 2 summarizes the aforementioned PSLs from [30], by reporting the values of ϵ (corresponding to the horizontal accuracy requirement). In our work, we consider a range of ϵ values that covers the range of values of Tab. 2. Consequently, we selectively set $\epsilon = \{20, 16, 8, 4, 2\}$ m.

TABLE 2. Uncertainty Localization Level ϵ for Different Positioning Service Levels (PSLs) [30].

Level index	Coverage	Deployment	ϵ
1	Indoor/Outdoor	Rural/Urban	20 m
2	Outdoor	Rural/Urban/Dense urban	6 m
{3,4,5,6}	Indoor/Outdoor	Rural/Urban/Dense urban	4 m

VII. RESULTS

A. REFERENCE SOLUTIONS

In order to position our approach, we consider the following reference approaches: *i*) beamforming with fixed widths, and *ii*) no beamforming. Focusing on *i*), we run S1-S8 of 5G-Pencil, by replacing S4 with a fixed width assignment. In particular, the beam widths are set equal to fixed angles $\alpha_{\text{FIXED}}^{\text{ST}}$, $\alpha_{\text{FIXED}}^{\text{TL}}$, which are retrieved from product data-sheets [26] and research works [10]. In this way, we assume to apply a "soft" beamforming, where localization is solely exploited to tune the beam direction, without tuning the beam widths in accordance with ϵ. Focusing on EMF and throughput evaluation, we employ the same models already introduced in Sec. III-C and Sec. III-D (with $\alpha_{(d,s)}^{\text{ST}} = \alpha_{\text{FIXED}}^{\text{ST}}$ and $\alpha_{(d,s)}^{\text{TL}} = \alpha_{\text{FIXED}}^{\text{TL}}$), in order to perform a fair comparison.

Regarding instead the case without beamforming, we introduce such term of comparison for EMF evaluation. More in depth, we assume that each gNB is realized with an omni-directional antenna, always radiating at the maximum power in all directions. As a consequence, both sectorization and beamforming are not employed in this case. More formally, we adopt a simplified version of the ITU point-source model to compute the PD that is received over each measurement

[5] 5G also includes sub-GHz and mm-Waves frequencies, which are however intentionally not treated in this work, due to the following reasons. First, it is expected that gNBs operating on sub-GHz frequencies will be mainly used for coverage. Therefore, the benefits of pencil beamforming will be limited in this case. Second, the installation of gNBs operating on mm-Waves is still at an early-stage in many contries, and mostly confined to specific scenarios (e.g., very dense areas). Consequently, in this work we focus on gNBs operating on mid-band frequencies, which are the currently adopted option for realizing 5G in many countries in the world (including Italy). The investigation of pencil beamforming with mm-Waves gNBs is left for future work.

[6] We intentionally neglect level 7 from our analysis, since the accuracy for such level is intended for relative positioning instead of absolute positioning.

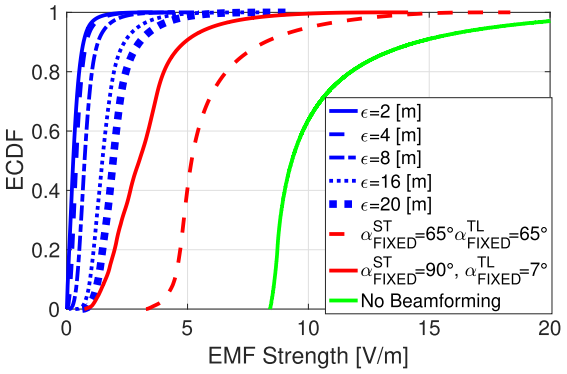

FIGURE 8. ECDF of the average EMF in each measurement spot by considering: *i*) pencil beamforming (for different values of localization uncertainty level ϵ), *ii*) beamforming with fixed widths and *iii*) no beamforming.

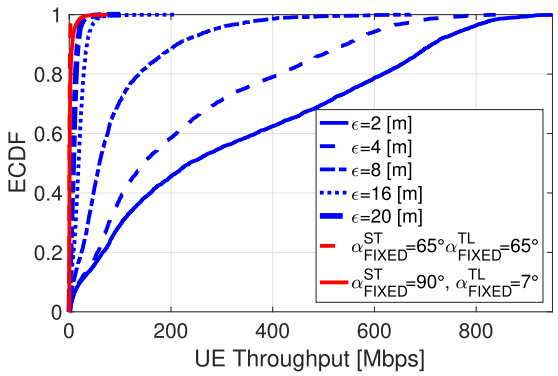

FIGURE 9. ECDF of the users throughput by considering: *i*) pencil beamforming (for different values of localization uncertainty level ϵ), *ii*) beamforming with fixed widths.

spot $m \in \mathcal{M}$:

$$S_m^{\text{TOT}} = \sum_g \frac{P_g^{\text{MAX}} \cdot G^{\text{MAX}}}{4\pi \cdot \delta_{(g,m)}^2} \tag{13}$$

where g is the considered gNB (belonging to the set of gNBs $\mathcal{G}$), $\delta_{(g,m)}$ is the 3D distance between gNB b and measurement spot m and P_g^{MAX} is the maximum radiated power by a 5G gNB (set to 200 [W] in accordance with [23]). Finally, the EMF strength is computed by applying Eq. (7). As a side comment, this setting represents a very conservative case, which may result in a potential large exposure over the covered area.

B. EMF AND THROUGHPUT COMPARISON

We initially evaluate the EMF exposure over each measurement point m of the central gNB. In this way, in fact, the total EMF results from the exposure of the central gNB plus the one from the six neighboring ones. In addition, we consider 20 independent runs for generating the coordinates of deployment spots in each sector s. We then run 5G-Pencil to compute E_m^{TOT} for each deployment spot generation, and then we compute the average of EMF over the 20 runs for each m. At the same time, we collect the throughput value for each deployment spot d that is served by the sectors of the central gNB. Unless otherwise specified, we assume NLOS conditions, and interference generated by the same sector (intra-sector term in Eq. 9) as well by the neighboring ones (inter-sector term in Eq. 9).

Fig. 8 reports the Empirical Cumulative Distribution Function (ECDF) from: pencil beamforming (with different ϵ values), beamforming with fixed widths, and no beamforming cases. Several considerations hold by analyzing in detail the figure. First, the pencil beamforming functionality triggers a strong decrease of EMF exposure compared to the reference solutions, thus contradicting the widespread belief of the population. In addition, the exposure tends to be further reduced as ϵ is decreased, due to the fact that narrower beam widths are synthesized. Eventually, the average exposure is overall pretty limited with pencil beamforming, with a maximum EMF almost equal to 5 [V/m], i.e., a value clearly lower than the limits defined by international regulations (e.g. International Commission on Non-Ionizing Radiation Protection (ICNIRP) ones [24]).

We now evaluate the throughput in terms of ECDF in Fig. 9. In this case, the throughput is evaluated under the most conservative settings, i.e., NLOS conditions and interference including the intra-sector term. Two considerations hold by analyzing the figure. First, pencil beamforming allows achieving consistently higher throughput values compared to beamforming with fixed widths. Obviously, this improvement derives from the reduction of interference terms in Eq. (9). In addition, the decrease of the localization uncertainty level ϵ results in a prompt increase of the throughput, with values even larger than 100 [Mbps] for more than 80% of the deployment spot (with ϵ=2 [m]). Therefore, we can conclude that pencil beamforming is beneficial not only in terms of EMF, but also for the throughput levels.

C. SPATIAL EXPOSURE ANALYSIS

We then move our attention to the characterization of pencil beamforming exposure over the territory. Fig. 10 reports a high-level quantitative analysis over one run, by showing the EMF strength and the number of overlapping beams, $\epsilon = \{20, 2\}$.[7] For this specific test, the same positioning of deployment spot is used $\epsilon = 20$ [m] and $\epsilon = 2$ [m]. Interestingly, we can note that, as the localization uncertainty level is improved, both the EMF exposure and the number of overalapping beams are reduced. This reduction is achieved not only for the measurement spots in proximity to the central gNB, but also over the whole sector extent. Therefore, when ϵ is decreased, the exposure over the territory tends to be reduced and in general uniformly distributed.

In the following step, we focus on the spatial evaluation of exposure over the deployment spots, which we remind are the zones of the territory which include UE. In more detail, we consider one generation of deployment spots. For each spot $d \in \mathcal{D}$, we compute the EMF as a linear average of

[7] To compute the overlapping beam metric, we assume a beam cone within the 3 [dB] zone, ending at point $I^N_{(d,s)}$.

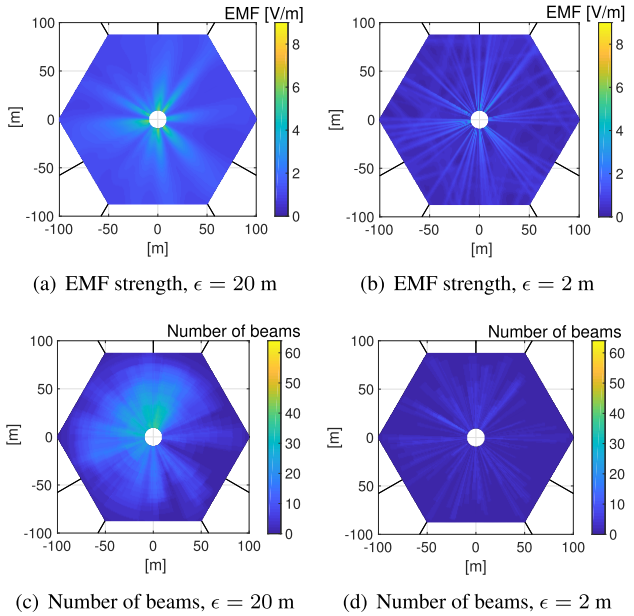

(a) EMF strength, $\epsilon = 20$ m (b) EMF strength, $\epsilon = 2$ m

(c) Number of beams, $\epsilon = 20$ m (d) Number of beams, $\epsilon = 2$ m

FIGURE 10. EMF strength and number of overlapping beams for $\epsilon = \{20, 2\}$ [m].

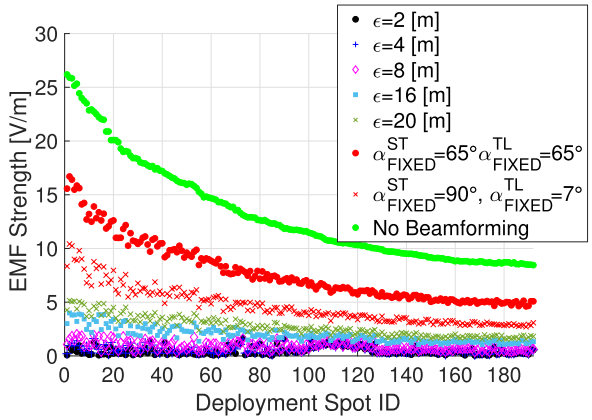

FIGURE 11. Average EMF in each deployment spot vs. deployment spot ID. The spots are ordered in decreasing distance w.r.t. serving sector.

the measurement spots falling in the circle centered in d of radius ϵ. We also introduce here the reference approaches, by computing the EMF for each d within a circle of radius $\epsilon = 2$ [m]. Fig. 11 reports the EMF strength vs. the deployment spots ID. Each ID is uniquely assigned by considering a sorting of the spots based on decreasing distance from the serving sector. By analyzing the figure, we can note that pencil beamforming allows reducing the exposure over the deployment spots. Clearly, such reduction is higher for those spots in proximity to the radiating gNB, i.e., those ones with lower IDs. In addition, the decrease of ϵ further reduces the exposure for all the spots w.r.t. the other reference solutions.

D. BEAM WIDTH FEASIBILITY

A natural question emerges at this point: Are the angles enforced by pencil beamforming overall feasible? To answer this question, Fig. 12 reports the average values and 95% confidence intervals of $\alpha^{\text{ST}}_{(d,s)}$ and $\alpha^{\text{TL}}_{(d,s)}$ (computed over the 20 runs, for all sectors) vs. the variation of ϵ. Interestingly, we can note that the beam widths tend to notably decrease as ϵ is reduced. In addition, the beam steering is always higher than the beam tilting (as expected). Clearly, the imposed angles are always higher than the minimum ones ($\alpha^{\text{ST}}_{\text{MIN}} = \alpha^{\text{TL}}_{\text{MIN}} = 3°$)

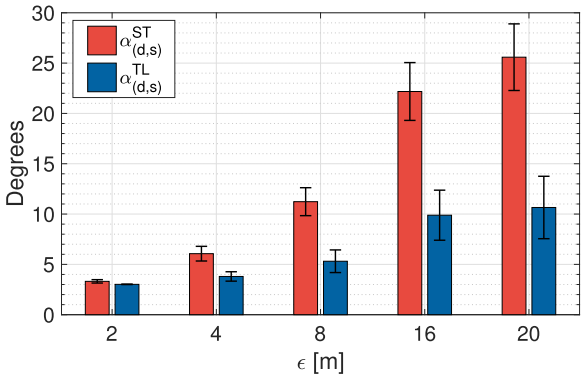

FIGURE 12. Average values and 95% confidence intervals for $\alpha^{\text{ST}}_{(d,s)}$ and $\alpha^{\text{TL}}_{(d,s)}$ vs. variation of localization uncertainty level ϵ.

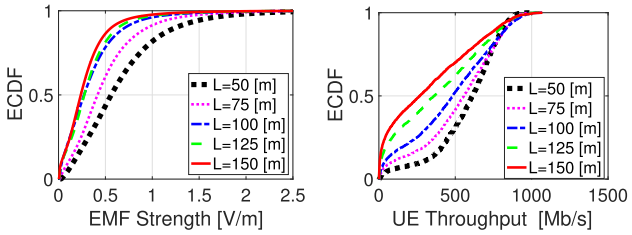

(a) EMF Evaluation (b) Throughput Evaluation

FIGURE 13. EMF and throughput evaluation vs. variation of sector size L (UE density decreasing with L).

E. IMPACT OF SECTOR SIZE AND UE DENSITY

In this part, we move our attention on the impact of pencil beamforming when the size of each sector (parameter L) *and* the UE density (i.e., number of deployment spots per sector over the sector area) are varied. To this aim, we consider the following cases: *i*) UE density increased with L, and *ii*) UE density kept constant w.r.t. L. Focusing on case *i*), we assume to always generate a number of deployment spots per sector equal to $N^{\text{R}}_s = 64$, i.e., the number of radiating elements. In this way, the UE density is reduced when L is increased. On the other hand, we impose a fixed UE density in case *ii*), i.e., the number of deployment spot per sector is proportional to the sector area, with a maximum value (i.e., equal to $N^{\text{R}}_s = 64$) achieved for the largest L. We then run 5G-Pencil for each setting, by assuming the following setting: *i*) only inter-sector interference (i.e., the intra-sector term in Eq. (9) is not considered), *ii*) $\epsilon = 2$ [m] and *iii*) 20 independent runs for generating the deployment spots.

Fig. 13 reports the ECDF of EMF and throughput for different values of L, by considering the case in which the UE density is decreasing with L. We remind that, with this setting,

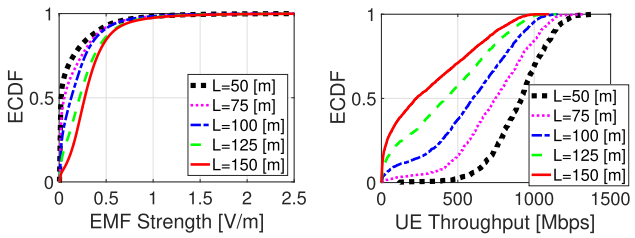

(a) EMF Evaluation (b) Throughput Evaluation

FIGURE 14. EMF and throughput evaluation vs. variation of sector size L (constant UE density).

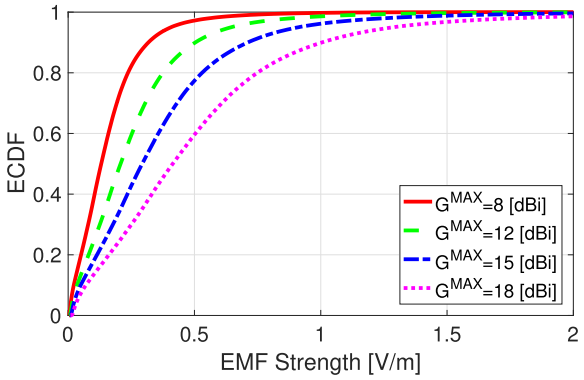

FIGURE 15. ECDF of the EMF strength vs. the variation of maximum antenna gain G^{MAX} with pencil beamforming ($\epsilon = 2$ [m]).

the number of deployment spots per sector is always equal to 64. Interestingly, the increase of L triggers a prompt decrease of EMF (Fig. 13(a)), due to the fact that the beam exposure overlapping is reduced (from both the same sector and the neighboring ones). In addition, the throughput tends to be decreased when L is increased (Fig. 13(b)), due to the larger distance (and hence worser propagation conditions) that is experienced by the deployment spot w.r.t. the serving sector.

We then move our attention to the investigation of EMF and throughput when the UE density is kept constant, as shown in Fig. 14. Interestingly, the EMF tends to be increased with L (Fig.14(a)), in contrast to the previous setting (Fig. 13(a)). However, we remind that in Fig. 14 we are increasing the number of deployed beams when L is increased, and therefore this setting introduces more radiating sources over the territory. In line with the previous case, the throughput is improved when L is decreased (Fig. 14(b)), thanks again to the shorter distance w.r.t. the serving sector. However, by comparing Fig. 14(b) and Fig. 13(b), the throughput is better in the former compared to the latter. Such difference is more evident for the lowest values of L. In this case, in fact, a reduced number of inter-sector interferers is introduced in Eq. (9), thus notably improving the observed throughput values.

F. IMPACT OF ANTENNA GAIN

In the final part of our work, we analyze the impact of the maximum antenna gain G^{MAX} that is used for the EMF evaluation. Fig. 15 reports the ECDF of the EMF obtained by 5G-Pencil for different values of G^{MAX}, by assuming again $\epsilon = 2$ [m] and 20 independent runs. As expected, the increase of G^{MAX} tends to increase the exposure levels. However, the EMF increase is overall pretty limited in terms of absolute value, with a maximum EMF strength always lower than 2 [V/m] for almost all the measurement spots.

VIII. SUMMARY AND FUTURE WORKS

We have investigated the impact of pencil beamfoming on EMF and throughput levels, by designing and evaluating the 5G-Pencil framework. Our solution, which operates as an upper layer on top of 5G core functionalities, leverages the localization uncertainty level to tune the direction and width for each traffic beam. We have then coded the presented framework as a publicly-released open-source simulator, in order to compute the EMF and the throughput of pencil beamforming in a meaningful set of scenarios. Our results demonstrate that the supposed EMF increase associated with pencil beamforming is not supported by scientific evidence. On the contrary, when the tuning of the traffic beams integrates localization information, a strong exposure reduction is observed not only over the deployment spots but also on the whole territory. In addition, the better is the localization uncertainty level, the narrower are the synthesized beams, and consequently the lower is the EMF exposure. Eventually, large throughput levels can be achieved when each deployment spot is served by one dedicated traffic beam.

As future work, we will consider the pencil beam activation/deactivation over space and over time, in order to minimize the exposure (while preserving the user Quality of Service). Such investigation will include e.g., power lock mechanisms to avoid exposure spikes. In addition, the adaptation of the traffic beams to track UE mobility over the territory is another avenue of research. Eventually, we will investigate the trade-off between the timing to synthesize a beam and the age of localization information, also in terms of exposure evaluation. Finally, we plan to extend our framework by considering pencil beams over mm-Waves frequencies.

ACKNOWLEDGMENT

The authors would like to thank Matteo Arciuli for his help in coding the initial version of the simulator.

REFERENCES

[1] *5G: A Dangerous Generation*. Accessed: Jan. 21, 2021. [Online]. Available: https://www.downtoearth.org.in/news/science-technology/5g-a-dangerous-generation-63802

[2] L. Chiaraviglio, A. Elzanaty, and M.-S. Alouini, "Health risks associated with 5G exposure: A view from the communications engineering perspective," 2020, *arXiv:2006.00944*. [Online]. Available: http://arxiv.org/abs/2006.00944

[3] *77 Cell Phone Towers Have Been Set Fire so Far Due to a Weird Coronavirus 5G Conspiracy Theory*. Accessed: Jan. 21, 2021. [Online]. Available: https://www.businessinsider.com/77-phone-masts-fire-coronavirus-5g-conspiracy-theory-2020-5?IR=T

[4] J. Bushberg, C. Chou, K. Foster, R. Kavet, D. Maxson, R. Tell, and M. Ziskin, "IEEE Committee on Man and Radiation - COMAR Technical Information Statement: Health and safety issues concerning exposure of the general public to electromagnetic energy from 5G wireless communications networks," *Health Phys.*, vol. 119, no. 2, p. 236, 2020.

[5] *Does 5G Pose Health Risks? (Part 2)*. Accessed: Oct. 22, 2020. [Online]. Available: https://www.edn.com/does-5g-pose-health-risks-part-2/
[6] *5G System (5GS) Location Services (LCS); Stage 2*, Standard Tech. Specification (TS) 23.273, Version 16.4.0, 3GPP, 3rd Generation Partnership Project (3GPP), Jul. 2020.
[7] W. Roh, J.-Y. Seol, J. Park, B. Lee, J. Lee, Y. Kim, J. Cho, K. Cheun, and F. Aryanfar, "Millimeter-wave beamforming as an enabling technology for 5G cellular communications: Theoretical feasibility and prototype results," *IEEE Commun. Mag.*, vol. 52, no. 2, pp. 106–113, Feb. 2014.
[8] B. Yu, L. Yang, and H. Ishii, "Load balancing with 3-D beamforming in macro-assisted small cell architecture," *IEEE Trans. Wireless Commun.*, vol. 15, no. 8, pp. 5626–5636, Aug. 2016.
[9] A. Awada, A. Lobinger, A. Enqvist, A. Talukdar, and I. Viering, "A simplified deterministic channel model for user mobility investigations in 5G networks," in *Proc. IEEE Int. Conf. Commun. (ICC)*, May 2017, pp. 1–7.
[10] A. Ali, U. Karabulut, A. Awada, I. Viering, O. Tirkkonen, A. N. Barreto, and G. P. Fettweis, "System model for average downlink SINR in 5G multi-beam networks," in *Proc. IEEE 30th Annu. Int. Symp. Pers., Indoor Mobile Radio Commun. (PIMRC)*, Sep. 2019, pp. 1–6.
[11] *Very Low' Risk of Unknown Health Hazards From Exposure to 5G Wireless Networks*. Accessed: Oct. 22, 2020. [Online]. Available: https://medicalxpress.com/news/2020-06-unknown-health-hazards-exposure-5g.html
[12] *5G Health—Ministry Health, New Zealand*. Accessed: Oct. 22, 2020. [Online]. Available: https://www.health.govt.nz/system/files/documents/topic_sheets/5g-and-health-aug19.pdf
[13] B. Thors, A. Furuskar, D. Colombi, and C. Tornevik, "Time-averaged realistic maximum power levels for the assessment of radio frequency exposure for 5G radio base stations using massive MIMO," *IEEE Access*, vol. 5, pp. 19711–19719, 2017.
[14] I. Nasim and S. Kim, "Adverse impacts of 5G downlinks on human body," in *Proc. SoutheastCon*, Apr. 2019, pp. 1–6.
[15] T. Basikolo, T. Yoshida, and M. Sakurai, "Electromagnetic field exposure evaluation for 5G in millimeter wave frequency band," in *Proc. IEEE Int. Symp. Antennas Propag. USNC-URSI Radio Sci. Meeting*, Jul. 2019, pp. 1523–1524.
[16] T. H. Loh, F. Heliot, D. Cheadle, and T. Fielder, "An assessment of the radio frequency electromagnetic field exposure from a massive MIMO 5G testbed," in *Proc. 14th Eur. Conf. Antennas Propag. (EuCAP)*, Mar. 2020, pp. 1–5.
[17] B. Xu, D. Colombi, and C. Tornevik, "EMF exposure assessment of massive MIMO radio base stations based on traffic beam pattern envelopes," in *Proc. 14th Eur. Conf. Antennas Propag. (EuCAP)*, Mar. 2020, pp. 1–5.
[18] S. Adda, T. Aureli, S. D'Elia, D. Franci, E. Grillo, M. D. Migliore, S. Pavoncello, F. Schettino, and R. Suman, "A theoretical and experimental investigation on the measurement of the electromagnetic field level radiated by 5G base stations," *IEEE Access*, vol. 8, pp. 101448–101463, 2020.
[19] *Location Services (LCS)*, Standard Tech. Specification (TS) 22.071, Version 16.0.0, 3GPP, 3rd Generation Partnership Project (3GPP), Jul. 2020.
[20] *Universal Geographical Area Description (GAD)*, Standard Tech. Specification (TS) 23.032, Version 16.0.0, 3GPP, 3rd Generation Partnership Project (3GPP), Jul. 2020.
[21] *ITU-T K70 Mitigation Techniques to Limit Human Exposure to EMFs in the Vicinity of Radiocommunication Station*. Accessed: Oct. 26, 2020. [Online]. Available: https://www.itu.int/rec/T-REC-K.70/en
[22] *ITU-T K.91: Guidance for Assessment, Evaluation and Monitoring of Human Exposure to Radio Frequency Electromagnetic*. Accessed: Oct. 26, 2020. [Online]. Available: https://www.itu.int/rec/T-REC-K.91-201911-I/en
[23] *Impact of EMF Limits on 5G Network Roll-Out*. Accessed: Oct. 27, 2020. [Online]. Available: https://www.itu.int/en/ITU-T/Workshops-and-Seminars/20171205/Documents/S3_Christer_Tornevik.pdf
[24] International Commission on Non-Ionizing Radiation Protection (ICNIRP), "Guidelines for limiting exposure to electromagnetic fields (100 kHz to 300 GHz)," *Health Phys.*, vol. 118, no. 5, pp. 483–524, May 2020. [Online]. Available: https://journals.lww.com/health-physics/FullText/2020/05000/Guidelines_for_Limiting_Exposure_to.2.aspx
[25] *5GPencil Simulator 1.1*. Accessed: Feb. 2, 2021. [Online]. Available: [Online]. Available: https://github.com/sarasaida/5GPencil
[26] *Hamilton 3.5 GHz* 8 × 8 *MIMO Panel Antenna*. Accessed: Oct. 27, 2020. [Online]. Available: https://halberdbastion.com/products/antenna-catalogue/hamilton-35-ghz-8x8-mimo-panel-antenna
[27] *Italian 5G Spectrum Auction*. Accessed: Jan. 15, 2021. [Online]. Available: https://5gobservatory.eu/italian-5g-spectrum-auction-2/
[28] *3GPP TR 38.901 Version 16.1.0 Release 16*. Accessed: Jan. 15, 2021. [Online]. Available: https://www.etsi.org/deliver/etsi_tr/138900_138999/138901/16.01.00_60/tr_138901v160100p.pdf
[29] *ITU-R SG05 Contribution 57: Guidelines for Evaluation of Radio Interface Technologies for IMT-2020*. Accessed: Jan. 15, 2021. [Online]. Available: https://www.health.govt.nz/system/files/documents/topic_sheets/5g-and-health-aug19.pdf
[30] *Service Requirements for the 5G System*, Standard Tech. Specification (TS) 22.261, Version 18.1.0, 3GPP, 3rd Generation Partnership Project (3GPP), Dec. 2020. .
[31] *Beamformers Explained*. Accessed: Jan. 20, 2021. [Online]. Available: https://www.commscope.com/globalassets/digizuite/542044-Beamformer-Explained-WP-114491-EN.pdf
[32] Z. L. Fazliu, F. Malandrino, C. F. Chiasserini, and A. Nordio, "MmWave beam management in urban vehicular networks," *IEEE Syst. J.*, early access, Jun. 8, 2020, doi: 10.1109/JSYST.2020.2996909.

LUCA CHIARAVIGLIO (Senior Member, IEEE) received the Ph.D. degree in telecommunication and electronics engineering from the Politecnico di Torino, Italy. He is currently an Associate Professor with the University of Rome Tor Vergata, Italy. He has coauthored over 140 papers published in international journals, books, and conferences. His current research interests include 5G networks, optimization applied to telecommunication networks, and health risks assessment of 5G communications. He is TPC Member of IEEE INFOCOM. He has received the Best Paper Award with the IEEE VTC-Spring 2020, the IEEE VTC-Spring 2016, and ICIN 2018. Some of his articles are listed as a Best Readings on Green Communications by IEEE. Moreover, he has been recognized as an author in the Top 1% most highly cited papers in the ICT field worldwide. He is an Associate Editor for *IEEE Communications Magazine* and IEEE TRANSACTIONS ON GREEN COMMUNICATIONS AND NETWORKING, and a Specialty Chief Editor of *Frontiers in Communications and Networks*.

SIMONE ROSSETTI received the bachelor's degree in Internet engineering from the University of Rome "Tor Vergata", Italy, in 2018, where he is currently pursuing the master's degree in ICT and Internet engineering. He is currently a Researcher with the Consorzio Nazionale Interuniversitario per le Telecomunicazioni (CNIT), Rome, Italy. He is involved in the European project H2020 LOCUS within the context of Localization and analytics for smart network management. His research interest includes 5G cellular network planning and analysis.

SARA SAIDA received the bachelor's degree in Internet technology engineering from the University of Rome "Tor Vergata", in 2018. She is currently pursuing the master's degree in ICT and Internet engineering with the University of Rome "Tor Vergata". She is currently working with the Consorzio Nazionale Interuniversitario per le Telecomunicazioni (CNIT) as a Researcher in the context of the European project H2020 LOCUS.

STEFANIA BARTOLETTI (Member, IEEE) received the Laurea degree *(summa cum laude)* in electronics and telecommunications engineering and the Ph.D. degree in information engineering from the University of Ferrara, Italy, in 2011 and 2015, respectively.

From 2016 to 2019, she was a Marie Skłodowska-Curie Global Fellow within the H2020 European Framework for a research project with the Massachusetts Institute of Technology and the University of Ferrara. She is currently a Researcher with the Institute of Electronics, Computer and Telecommunication Engineering (IEIIT), National Research Council of Italy (CNR), and an Associated Researcher of CNIT. Her research interest includes theory and experimentation of wireless networks for localization and vehicular communications.

Dr. Bartoletti was a recipient of the 2016 Paul Baran Young Scholar Award of the Marconi Society. She is currently an Editor of the IEEE COMMUNICATIONS LETTERS. She served as the Chair of the TPC for the IEEE International Conference on Communications Workshop on Advances in Network Localization and Navigation (ANLN), from 2017 to 2020.

NICOLA BLEFARI-MELAZZI is currently a Full Professor of telecommunications with the University of Rome "Tor Vergata", Italy. He is also the Director of CNIT, a consortium of 37 Italian Universities. He has participated in over 30 international projects. He has been a Principal Investigator of several EU funded projects. He has been an Evaluator for many research proposals and a Reviewer for numerous EU projects. He is the author/coauthor of about 200 articles, in international journals and conference proceedings. His research interests include the performance evaluation, design and control of broadband integrated networks, wireless LANs, satellite networks, and the Internet.